

for carrying out spectroscopic calculations on the oxygen transitions, and R. A. Copeland for his contributions. The W. M. Keck Observatory is operated by the California Institute of Technology and the University of California. D.E.O. and J.P.F. acknowledge NSF for par-

tial support of this research under grant AST 91-23547. T.G.S. and D.L.H. acknowledge support by NASA Space Physics Division under grant NAGW-3669.

14 February 1997; accepted 17 July 1997

Detection of Soft X-rays and a Sensitive Search for Noble Gases in Comet Hale-Bopp (C/1995 O1)

Vladimir A. Krasnopolsky,* Michael J. Mumma, Mark Abbott, Brian C. Flynn, Karen J. Meech, Donald K. Yeomans, Paul D. Feldman, Cristiano B. Cosmovici

An image of comet Hale-Bopp (C/1995 O1) in soft x-rays reveals a central emission offset from the nucleus, as well as an extended emission feature that does not correlate with the dust jets seen at optical wavelengths. Neon was found to be depleted in the cometary ice by more than a factor of 25 relative to solar abundance, which suggests that ices in Hale-Bopp formed at (or later experienced) temperatures higher than 25 kelvin. A helium line emission at a wavelength of 584 angstroms was detected and may be attributable to charge transfer of solar wind α particles in the cometary coma. Ionized oxygen and another helium line contribute to an emission observed at 538 angstroms.

The Extreme Ultraviolet Explorer satellite (EUVE) provides spectroscopic measurements of celestial objects in a wavelength range of 70 to 760 Å and imaging in a 70 to 180 Å (\approx 180 to 70 eV) bandpass (1). At 760 Å, the photon energy (16.3 eV) exceeds the bond energies in molecules and the ionization potentials of most neutral atoms (except He, Ne, and F); hence, only spectral lines of He, Ne, F, and atomic ions are expected in the extreme ultraviolet (EUV) spectra of comets. He and Ne have resonance lines in this range, and abundances of Ne could serve to constrain the temperature at which precometary ices formed. Only upper limits to abundances of He, Ne, and Ar have been established in comets (2), but those for Ne and Ar exceeded the solar abundances by more than an order of magnitude. Solar light is faint in the EUV, so even the strongest EUV emissions from bodies such as the moon, Mars, and Jupiter are near the detection limit (3).

Hale-Bopp (C/1995 O1) is perhaps the biggest and brightest comet of this century; its nucleus mass may exceed that of comet 1P/Halley by a factor of 40 (4). Our EUVE observation of Hale-Bopp was acquired from 14 to 19 September 1996, when the comet was at heliocentric and geocentric distances $r = 3.07$ AU and $\Delta = 2.91$ AU, respectively. The total exposure time was 1.4×10^5 s, and its effective value was reduced to $\tau = 9 \times 10^4$ s as a result of filtering (5).

A soft x-ray image of Hale-Bopp in the range of 70 to 180 eV was obtained and corrected for background and for a known vignetting function (6). To improve the signal-to-noise ratio, we convolved the image with a Gaussian having a radius at half-maximum of 1.5×10^5 km (Fig. 1A). An optical image (Fig. 1B), enhanced to show dust jets more clearly (7), does not correlate with the x-ray image. The x-ray

emission is not centered on the expected position of the nucleus. The center of brightness is offset relative to the expected position of the nucleus by $1.4 (\pm 0.6) \times 10^5$ km in the sky plane. If the brightness center lies on the sun's azimuth, then the distance of the brightness center from the nucleus is $2.7 (\pm 1.2) \times 10^5$ km (8). The center of brightness is between the radius vector to the sun and the comet velocity vector, and an extended region of emission is seen toward the southwest. A weak feature in the antiveloc direction is also seen.

The soft x-ray brightness varies with distance from the brightness center ρ_0 (Fig. 2). The x-ray brightness in Hale-Bopp is maximum at 0.005 rayleighs and decreases by a factor of 3 to $\rho_0 = 2 \times 10^5$ km. The production rate of x-ray photons Q_x is $8 (\pm 2) \times 10^{24}$ photons s^{-1} for $\rho_0 = 4 \times 10^5$ km (9, 10) (Fig. 3). If charge transfer is a dominant excitation process, then [using a spectrum from (10) and our measurement] we expect a total x-ray ($E > 80$ eV) luminosity of 3.5×10^{25} and 2.6×10^{25} photons s^{-1} for $\rho = 4 \times 10^5$ and 2.5×10^5 km, respectively.

The Ne 736 Å line is traditionally used as a tool to search for Ne. However, the second resonance line for Ne (the analog of Lyman- β) at 630 Å coincides with a strong emission line in the solar spectrum and therefore provides better detection prospects than the 736 Å line, by two orders of magnitude (12). The advantage of the 630 Å line reaches three orders of magnitude for EUVE, which has a lower efficiency at 736 Å than at 630 Å.

No cometary signal is seen at 630 Å, and a 2σ upper limit corresponds to 45 counts for the largest bin (Fig. 4); this limit corresponds to $Q_{Ne} < 4 \times 10^{27} s^{-1}$ (13). The production rate of oxygen (as H_2O , CO, and CO_2) was equal to $6.6 \times 10^{29} s^{-1}$ during the observation (4). Hence, the Ne/O ratio in the gas alone is $< 6 \times 10^{-3}$ in Hale-Bopp. The ratio of oxygen in the dust and gas was 1.3 in comet 1P/Halley (14). Scaling to the dust and gas productions in both comets (4, 15), we find that this ratio is ~ 8 in Hale-

V. A. Krasnopolsky, Catholic University of America, Washington, DC 20064, USA, and NASA Goddard Space Flight Center, Greenbelt, MD 20771, USA.

M. J. Mumma, NASA Goddard Space Flight Center, Greenbelt, MD 20771, USA.

M. Abbott and B. C. Flynn, Center for Extreme Ultraviolet Astrophysics, Berkeley, CA 94720, USA.

K. J. Meech, Institute for Astronomy, Honolulu, HI 96822, USA.

D. K. Yeomans, Jet Propulsion Laboratory, Pasadena, CA 91109, USA.

P. D. Feldman, Johns Hopkins University, Baltimore, MD 21218, USA.

C. B. Cosmovici, Istituto Fisica Spazio Interplanetario, CNR, 00044 Frascati, Italy.

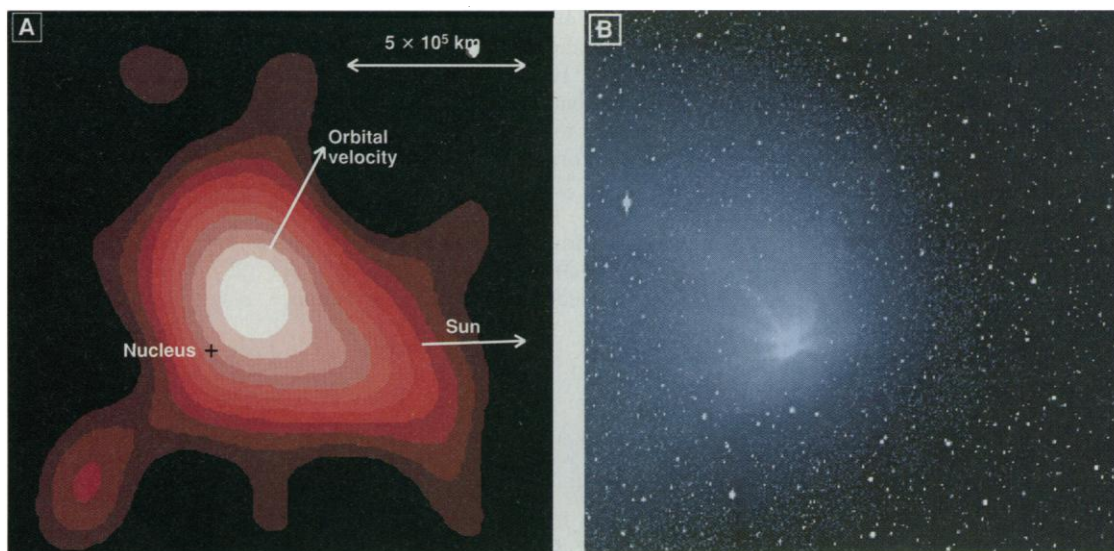
*To whom correspondence should be addressed (at NASA). E-mail: ys2VK@lepvax.gsfc.nasa.gov

Table 1. Observations of soft x-rays in Hyakutake and Hale-Bopp. X-ray data for Hyakutake are from (37); r is the heliocentric distance, Q_x is the x-ray photon production rate observed within a cometary radius ρ_0 , ρ_B is the offset of the brightness center from the nucleus, Q_{gas} is the gas production rate (4, 38), and A/r_p is proportional to the dust production rate (4, 38). $A/r_{p,x}$ is discussed in (35).

Parameter	Hyakutake	Hale-Bopp
r (AU)	1.07	3.07
Q_x (photons s^{-1})	$1 (\pm 0.2) \times 10^{26}$ *	$8 (\pm 2) \times 10^{24}$
ρ_0 (km)	1.2×10^5	4×10^5
ρ_B (km)	$5.6 (\pm 1) \times 10^4 \dagger$	$2.7 (\pm 1.2) \times 10^5$
Q_{gas} (s^{-1})	2×10^{29}	6×10^{29}
A/r_p (m)	79	630
$(A/r_{p,x})$ (m)	3700	7500
$(A/r_{p,x})/A/r_p$	47	12

* 10^{26} photons s^{-1} from (34). † 3×10^4 km from (34).

Fig. 1. (A) EUVE image of Hale-Bopp at photon energies of 70 to 180 eV (soft x-rays). The directions to the sun and of the comet's orbital velocity, projected onto the sky plane, are shown. North is at the top and east is to the left. (B) Optical image of Hale-Bopp on 16 September 1996, with same orientation and scale as in (A). An azimuthally averaged brightness has been subtracted from the original image to enhance the contrast on the dust jets. The dust jets are not seen in the x-ray image, and an extended feature in x-rays is not seen in the optical image.



Bopp (which is very dusty) if the dust properties (density, composition, size distribution) are the same in these two comets. We then estimate $\text{Ne}/\text{O} < 7 \times 10^{-4}$ in the bulk nucleus of Hale-Bopp. In comparison with the solar ratio of $\text{Ne}/\text{O} = 0.15$ (16), the Ne in Hale-Bopp is depleted relative to the solar abundance by factors of more than 25 and 200, respectively, in the ice and in the sum of ice and dust.

Laboratory studies demonstrate that Ne is trapped efficiently in water ice only at temperatures below 25 K (17). Even if trapped in icy grain mantles, Ne can only be retained if the ices remain at sufficiently low temperatures, owing to the high mobility of noble gases in an ice matrix. Warming to higher temperatures (~ 50 K) will permit Ne to escape while less mobile species trapped in water ice (for example, C_2H_6 and CO) are retained. Thus, the Ne abundance tests the maximum temperature to which

precometary ices were exposed before incorporation into comets. Laboratory measurements cannot duplicate the long time scales experienced by ices in the natal cloud core (up to 10^7 years) or in the solar nebula, so their use as guides is uncertain in this aspect. However, the observed temperature dependence of the ability of the ice to trap gas as it forms should be more certain. Our nondetection of Ne agrees with predictions (18) that were based on the laboratory data.

Hale-Bopp is an Oort cloud comet, and the absence of Ne is consistent with the current view that Oort cloud comets formed in the Jupiter-Neptune region of the solar nebula (19) where temperatures exceeded 50 K. Kuiper belt comets formed in the trans-Neptunian region and some may incorporate a solar abundance of neon ($\text{Ne}/\text{O} = 0.15$), because nebular temperatures in

that region could have been < 25 K.

An emission line was detected in the long-wavelength (LW) spectrum near 538 Å (Fig. 4) with a photon production rate of 5.2×10^{25} photons s^{-1} for $\rho = 2.5 \times 10^5$ km (13), possibly from O^+ 538/39 Å or He 537 Å. Excitation of O^+ 538/39 Å proceeds by photoionization of neutral O and OH by solar photons with $\lambda < 339$ Å and 303 Å, respectively. Emission rate factors are equal to 2.3×10^{-9} and 1.2×10^{-9} photons s^{-1} atom $^{-1}$, respectively (20). Our calculations show that O^+ 538/39 Å could explain 60% of the observed emission. The rest may be attributable to the He 537 Å line.

The He 584 Å line is seen in all spectra (Fig. 4). Geocoronal extinction at 584 Å is negligible at the comet's geocentric velocity of 9.6 km s^{-1} (21). The difference (Fig. 5, C and D) between the LW spectrum near 584 Å

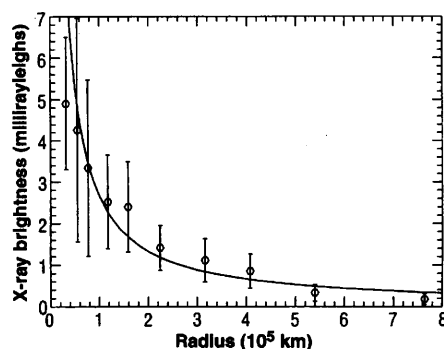


Fig. 2. Mean brightness of Hale-Bopp in soft x-rays as a function of distance from the brightness center. The function A/r is also shown (solid line); this function describes the brightness distribution expected for dust and gaseous parent molecules. One rayleigh corresponds to a column production of 10^6 photons $\text{cm}^{-2} \text{s}^{-1}$ (4π ster) $^{-1}$.

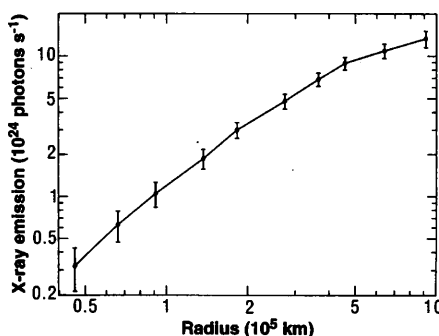


Fig. 3. Total x-ray emission of Hale-Bopp as a function of aperture (radius). A slope α of the function corresponds to a power index in $Q_x = A\rho_0^\alpha$. The value of α varies from 2 at $\rho_0 = 0.5 \times 10^5$ km to 0.6 at 7×10^5 km; $\alpha = 2$ is expected if the x-ray intensity is proportional to the local solar wind flux alone (collisionally thick case), and $\alpha = 1$ is expected if the x-ray intensity is proportional to the column density of gas or dust for spherically symmetric uniform outflow.

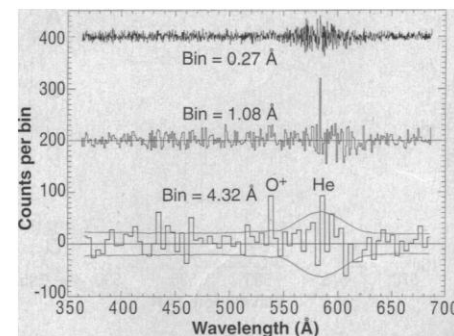


Fig. 4. LW EUVE spectra of Hale-Bopp at 370 to 680 Å for various bin sizes. The comet is too faint to be detected by the SW spectrometer (11). The LW spectra were extracted in bins of $540,000 \times 23,000$ km (upper trace), $540,000 \times 90,000$ km (middle trace), and $540,000 \times 360,000$ km (lower trace), corrected for the background. The signal-to-noise ratio is equal to 3.8 for the He 584 Å line in the middle spectrum. Ordinates of the upper and middle traces are shifted for convenience.

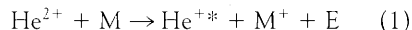
(Fig. 5A) and the background (Fig. 5B) shows the presence of the He line with a production rate of 1.2×10^{26} photons s^{-1} for $\rho = 2.5 \times 10^5$ km. Neon is absent in the nucleus, and this means that helium—the most mobile and volatile gas—cannot be retained in the nucleus. Helium probably appears in the comet because of charge transfer from solar wind α -particles to cometary neutrals.

No emission was observed in the medium-wavelength (140 to 380 Å) spectrum, and a 2σ upper limit for the production of He⁺ 304 Å photons is 7×10^{25} photons s^{-1} for $\rho = 2.5 \times 10^5$ km. According to statistics, the counts in two bins in the bottom spectrum in Fig. 4 should exceed a 2σ level even if no real emission is present. Probably, these are the bins at 465 and 435 Å.

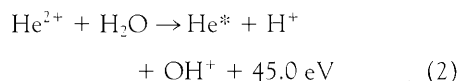
Observations of the He and He⁺ lines may be a diagnostic tool to study interaction of the solar wind with comets. Charge transfer excitation of He is similar to that of x-rays (10, 22, 23). Therefore, we compare the measured cometary photon production rates of three lines for $\rho = 2.5 \times 10^5$ km: 1.2×10^{26} photons s^{-1} for He 584 Å, 2×10^{25} photons s^{-1} for He 537 Å, and $<7 \times 10^{25}$ photons s^{-1} for He⁺ 304 Å.

Two excitation processes may be considered for these emissions: resonant scattering of solar photons by He and He⁺, and prompt excitation in two- and one-electron captures by solar wind α -particles. Resonant scattering emission rate factors are equal to 7.5×10^{-6} photons s^{-1} atom⁻¹ for 584 Å, 1.3×10^{-7} photons s^{-1} atom⁻¹ for 537 Å, and 2.3×10^{-5} photons s^{-1} atom⁻¹ for 304 Å, at 1 AU for solar minimum (24). If He were ejected from the nucleus, then its resonant scattering would correspond to He/O

$= 3 \times 10^{-4}$ in cometary gas and 4×10^{-5} in gas and dust, that is, depleted by factors of 2×10^{-6} and 3×10^{-7} relative to the solar abundance. However, even these values are too high and incompatible with the laboratory data (17). One-electron capture,



is a nearly resonant process for excitation of He⁺ 304 Å with a yield of ~ 0.5 (25). Two-electron capture, for example



is weaker than one-electron capture by a factor of 2 (26). A yield of He 584 Å may be $\sim 1/3$ in this process (27). These values favor a total charge transfer rate of $\sim 2 \times 10^{26}$ s^{-1} for α -particles and negligible contributions of resonant scattering to He 537 Å and He⁺ 304 Å. Resonant scattering is a main process for He 584 Å (28).

Of the many processes proposed for the excitation of cometary x-rays (10, 22, 23, 29, 30), charge transfer of solar wind heavy ions (10, 22, 23) and scattering of solar x-rays by small (10^{-19} g) dust particles (23, 29) seem to be the most promising. Charge transfer excites x-rays and He emissions. Cross sections for heavy ions exceed those for α -particles by a factor of 10 to 30 in this process (31), and the x-ray luminosity expected for linear scaling of this process is $20 \times (2 \times 10^{26})/35 \approx 10^{26}$ photons s^{-1} for $\rho = 2.5 \times 10^5$ km (35 is the ratio of α -particles to heavy ions in the solar wind). This value is even higher than the total x-ray ($E > 80$ eV) luminosity of 2.6×10^{25} photons s^{-1} obtained from our measurement. However, both the brightness offset $\rho_B = 2.7 \times 10^5$ km and the slope $\alpha \approx 2$ (Fig. 3) favor collisionally thick conditions for the solar wind, with a deviation of a factor of $b = 2$ from these conditions at $\rho = 2.5 \times 10^5$ km (Fig. 3); then the linear scaling is not valid, and the expected total x-ray ($E > 80$ eV) luminosity is 3×10^{25} photons s^{-1} (32). The excellent agreement between this estimate and our measured x-ray luminosity suggests charge transfer as the dominant process of x-ray excitation.

Comparison of the distances ρ_B between the brightness center and the nucleus in Hale-Bopp and Hyakutake (Table 1) may also be used to resolve this question. If small dust particles are responsible for the emission and they are ejected directly from the nucleus, then the displacement of the brightness center is related to the direction of dust ejection, to dust velocity, to the effects of solar radiation pressure on dust, and to the charging of small dust particles and their removal by electromagnetic forces. The displacement should be proportional to r^α with $\alpha = 1$ to 1.5 (33)

and does not depend on the absolute production rate for dust; the observed displacement ratio of 4.8 ± 2.3 agrees with the expected value of 3 to 5. If charge transfer is responsible for x-rays, then molecular column abundances from the brightness center to infinity, $N = Q_{\text{gas}}/(4\pi\rho_B v)$, should be the same for both comets. We take the velocity as in (13) and the Q_{gas} rates from Table 1, so the displacement ratio is 5 for this process. Both scattering by small dust and charge transfer with cometary dust agree with the measured displacement ratio (34).

The relative production rates of x-rays in Hale-Bopp and Hyakutake may also be used to identify the excitation process. Ratios of the dust-scattering factors A_{fp} in the x-ray spectrum (35) to those in the visible spectrum differ by a factor of 4 (Table 1), and this does not favor small dust scattering. If small particles are "glued" into large grains by icy or organic refractory material, then the higher dust temperatures at 1 AU (~ 325 K) compared with those at 3.1 AU (~ 190 K) may lead to higher production efficiencies for very small dust and may explain the difference. If charge transfer is the main excitation process, then the efficiencies of this excitation in Hale-Bopp and Hyakutake differ only by a factor of 1.5 (36). This small difference and our observation of helium favors the charge transfer mechanism.

REFERENCES AND NOTES

1. S. Bowyer and R. F. Malina, in *Extreme Ultraviolet Astronomy*, R. F. Malina and S. Bowyer, Eds. (Perigamon, New York, 1991), pp. 397–408. EUVE has imaging instruments that cover the entire spectral range of 70 to 760 Å. However, only imaging at 70 to 180 Å with the Deep Survey camera (DS) can be used simultaneously with the spectrometers.
2. S. A. Stern, J. C. Green, W. Cash, T. A. Cook, *Icarus* **95**, 157 (1992); P. D. Feldman *et al.*, *Astrophys. J.* **379**, L37 (1991).
3. V. A. Krasnopolsky, S. Bowyer, S. Chakrabarti, G. R. Gladstone, J. S. McDonald, *Icarus* **109**, 337 (1994); G. R. Gladstone, J. S. McDonald, W. T. Boyd, S. Bowyer, *Geophys. Res. Lett.* **21**, 461 (1994); G. R. Gladstone, D. T. Hall, J. H. Waite Jr., *Science* **268**, 1595 (1995).
4. The nucleus size is suggested to be 35 ± 7 km (39). The gas and dust production rates during EUVE observations of Hale-Bopp were $Q_{\text{H}_2\text{O}} = 2.1 \times 10^{29}$ s^{-1} , $Q_{\text{CO}_2} = 8.8 \times 10^{28}$ s^{-1} , and $A_{\text{fp}} = 2100$ m (39); $Q_{\text{H}_2\text{O}} = 3.6 \times 10^{29}$ s^{-1} and $Q_{\text{CO}} = 1.7 \times 10^{29}$ s^{-1} [from radio observations; N. Biver *et al.*, *Science* **275**, 1915 (1997)]; $Q_{\text{H}_2\text{O}} = 3.3 \times 10^{29}$ s^{-1} , $Q_{\text{CO}} = 2.3 \times 10^{29}$ s^{-1} , and $Q_{\text{CO}_2} = 0.74 \times 10^{29}$ s^{-1} (from the Infrared Space Observatory; J. Crovisier *et al.*, *ibid.*, p. 1904); $Q_{\text{H}_2\text{O}} = 3 \times 10^{29}$ s^{-1} and $A_{\text{fp}} = 7 \times 10^4$ cm (from multiband optical photometry; D. G. Schleicher, S. M. Lederer, R. L. Millis, T. L. Farnham, *ibid.*, p. 1913); and $A_{\text{fp}} = 5.6 \times 10^4$ cm (H. Rauer *et al.*, *ibid.*, p. 1909). A_{fp} , a photometric parameter related to the dust production rate in comets, is a product of the dust albedo A , filling factor f , and a diaphragm radius (distance from the nucleus) ρ to which this factor refers (40) [M. F. A'Hearn, D. G. Schleicher, P. D. Feldman, R. L. Millis, D. T. Thompson, *Astron. J.* **89**, 579 (1984)].
5. In analysis we present here, the measured photon and background counts were remapped with corrections for cometary motion on the celestial sphere, the changing comet-sun direction, the EUVE orbital parallax, and the

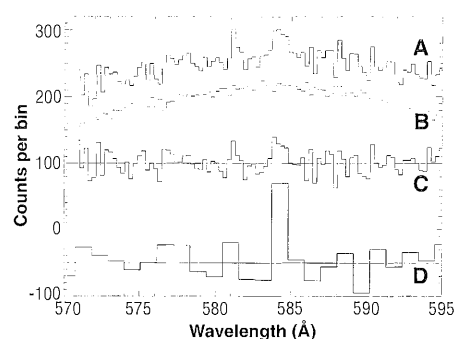


Fig. 5. A portion of the LW spectrum, showing the presence of the He 584 Å line. (A) Sum of 60 central rows on the detector (signal + background, the spectrum of the comet in a bin of $540,000 \times 23,000$ km). (B) Sum of 540 rows above and below the central rows divided by 9 (background, obtained from positions off the comet). (C) The difference of (A) and (B). (D) Same as (C), but binned by four pixels in the dispersion direction. Ordinates of (A), (C), and (D) are shifted by 50, 100, and -50 counts per bin for convenience.

changes in the telescope pointing direction during the observation. The detected photon list was filtered to remove times when EUVE was in the South Atlantic Anomaly (which causes high background levels) and occultations by the Earth's limb below tangent altitudes of 200 km.

6. The optical filters used for DS and the short-wavelength (SW) spectrometer are not completely opaque to photons outside the nominal instrument range, that is, they have some nonzero transmission at longer wavelengths. The resulting effective area of the DS is 10^{-8} , 10^{-7} , and 10^{-9} of the peak value (28 cm^2 at 140 eV) at 1216 , 2500 , and 3090 \AA , respectively [K. McDonald *et al.*, *Astron. J.* **108**, 1843 (1994)]. Therefore, some contribution to the image is expected from cometary H 1216 \AA and OH 3090 \AA wavelength emissions and from dust scattering at 2600 to 3300 \AA . Calculations of the leak signal were made on the basis of known H_2O and dust production rates, scale lengths, and velocities (47) [P. D. Feldman *et al.*, *Astron. Astrophys.* **187**, 325 (1987)]. The calculated leak signal is equal to 6% of the measured value for $\rho < 5 \times 10^4 \text{ km}$ and 3% for $\rho < 3 \times 10^5 \text{ km}$; the proper corrections have been done.
7. The optical image was obtained on 16 September 1996 with the University of Hawaii 8192 \times 8192 mosaic camera at the Canada-France-Hawaii telescope prime focus. The plate scale is $0.206 \text{ arc sec per pixel}$. The image is stored as eight 2048×4096 images. The mosaic was assembled astrometrically by performing a plate solution for each frame with the use of the Monet astrometric catalog of the digital sky survey and software developed by M. Buie at Lowell Observatory. Because each of the detectors has a different gain, the mosaic was normalized to the gain for the detector in the northwest corner.
8. The sun-comet-Earth angle was 19° . The EUVE position uncertainty, caused by thermal flexure of the spacecraft, is 30 arc sec [M. J. Abbott *et al.*, *Astrophys. J. Suppl. Ser.* **107**, 451 (1996)].
9. This value of Q_x , and Figs. 2 and 3, refer to the effective instrument bandpass of 95 to 165 eV and were calculated for a spectrally uniform emission. The photon production rate may also be given as $1.15 (\pm 0.3) \times 10^{23} \text{ photons s}^{-1} \text{ eV}^{-1}$.
10. Three lines dominate in x-ray emission in the DS spectral range [R. M. Häberli, T. I. Gombosi, D. L. De Zeeuw, M. R. Combi, K. G. Powell, *Science* **276**, 939 (1997)]. Assuming their intensity distribution, our measurements correspond to $1.2 \times 10^{25} \text{ photons s}^{-1}$ at $\text{O}^{5+} 83 \text{ eV}$, $7.5 \times 10^{24} \text{ photons s}^{-1}$ at $\text{O}^{6+} 96 \text{ eV}$, and $2 \times 10^{24} \text{ photons s}^{-1}$ at $\text{Ne}^{7+} 141 \text{ eV}$.
11. The EUVE spectrometers are of objective-grating type with two-dimensional position-sensitive detectors having 2048×2048 pixels (7). The EUVE SW spectrometer provides a spectrum of Hale-Bopp in a range of 70 to 190 \AA . We used rectangular bins with a size of $900,000 \times 800,000 \text{ km}$ and 2.3 \AA in dispersion to improve the signal-to-noise ratio; however, no signal exceeding a 2σ level of 80 counts was observed. The DS signal is equal to 1000 counts in the same sky aperture, and the expected signal in the full SW range is just $1000 \times 2/28 = 70$ counts. Here, 2 and 28 cm^2 are the effective areas of the SW and DS, respectively. We cannot detect Hale-Bopp with the SW spectrometer even if the total x-ray emission were concentrated in a single line.
12. The wavelength of this line, 629.7388 \AA [R. L. Kelly, *J. Phys. Chem. Ref. Data* **16** (suppl. 1), 1 (1987)], coincides with the OV line at 629.732 \AA , which is among the strongest emissions in the solar spectrum. Its intensity is equal to $1.59 \times 10^9 \text{ photons cm}^{-2} \text{ s}^{-1}$ at solar minimum (42). A $1/e$ half-width of the OV 630 \AA line is equal to 85 m\AA (G. J. Rottman, personal communication). The oscillator strength of the Ne 630 \AA line is $f = 0.0086$ (43), and the emission rate factor at solar minimum is

$$g_{630 \text{ \AA}} = 2.5 \times 10^{-7} \times \exp \left[- \left(\frac{v_h + 8}{v_0} \right)^2 \right] \text{ photons s}^{-1} \text{ atom}^{-1} \quad (3)$$

where v_h is the comet's heliocentric velocity in kilometers per second, $v_0 = 40 \text{ km s}^{-1}$ is the OV linewidth in terms of Doppler velocity, and 8 km s^{-1} is the sum of corrections for the wavelength difference of 3 km s^{-1} and a downward velocity of solar OV ions of 5 km s^{-1} [P. Brekke, *Astrophys. J.* **408**, 735 (1993)]. The cal-

culated g factor has been corrected for the near-infrared transitions from the upper level.

13. The observed signal (<45 counts) is $S = (g\rho Q_A\tau)/(8v\Delta^2a^2)$. We assume a gas outflow velocity of $v = 0.85/r^{1/2} \text{ km s}^{-1}$ [A. Cochran and D. G. Schleicher, *Icarus* **105**, 235 (1993)] and apply $g_{630 \text{ \AA}} = 2.4 \times 10^{-8} \text{ photons s}^{-1}$ for $r = 3.07 \text{ AU}$ and $v_h = -20 \text{ km s}^{-1}$. The instrument effective area is $A = 0.13 \text{ cm}^2$ at 630 \AA , 0.37 cm^2 at 538 \AA , 0.18 cm^2 at 584 \AA , and 0.41 cm^2 at 304 \AA ; $a = 1.5 \times 10^{13} \text{ cm}$ is the astronomical unit (the sun-Earth distance).
14. E. K. Jessberger and J. Kissel, in *Comets in the Post-Halley Era*, R. Newburn, M. Neugebauer, J. Rahe, Eds. (Kluwer Academic, Dordrecht, Netherlands, 1991), pp. 1075–1092.
15. $Q_{\text{gas}} \approx 10^{30} \text{ s}^{-1}$ in 1P/Halley during the Vega 2 flyby (39) [V. A. Krasnopolsky, A. Yu. Tkachuk, O. I. Korablev, *Astron. Astrophys.* **245**, 662 (1991); K. I. Gringauz and M. I. Verigin, in *Comet Halley: Investigations, Results, Interpretations*, J. W. Mason, Ed. (Ellis Horwood, New York, 1990), pp. 147–163; H. A. Weaver, M. J. Mumma, H. P. Larson, *Astron. Astrophys.* **187**, 411 (1987)], and $Afp = 170 \text{ m}$ (38). The Vega 2 flyby was between Vega 1 and Giotto and is therefore chosen.
16. E. Anders and N. Grevesse, *Geochim. Cosmochim. Acta* **53**, 197 (1989).
17. A. Bar-Nun and D. Priainik, *Astrophys. J.* **324**, L31 (1988).
18. T. Owen and A. Bar-Nun, *Icarus* **116**, 215 (1995).
19. V. S. Safronov, *Evolution of the Protoplanetary Cloud and Formation of the Earth and Planets* (Nauka, Moscow, 1969); *NASA Tech. Transl. TT-F-677* (1972); M. J. Mumma, P. R. Weissman, S. A. Stern, in *Protostars and Planets III*, E. H. Levy and J. I. Lunine, Eds. (Univ. of Arizona Press, Tucson, 1993), pp. 1172–1252.
20. The $\text{O}^+ 834 \text{ \AA}$ emission in the terrestrial dayglow is excited by the same process. Its emission rate factor is equal to $9 \times 10^{-9} \text{ photons s}^{-1} \text{ atom}^{-1}$ at solar minimum (42). The dayglow emission at $538/39 \text{ \AA}$ is weaker than that at 834 \AA by a factor of 4 in optically thin conditions [S. Chakrabarti, F. Paresce, S. Bowyer, R. Kimble, *J. Geophys. Res.* **88**, 4898 (1983)]; its emission rate factor is then $2.3 \times 10^{-9} \text{ photons s}^{-1} \text{ atom}^{-1}$. We assume the same yield of this emission for OH and O. Resonant scattering of $\text{O}^+ 539 \text{ \AA}$ is inefficient because of the low solar intensity at this wavelength and low O^+ densities in comets [K. Altwegg *et al.*, *Astron. Astrophys.* **279**, 260 (1993)].
21. V. A. Krasnopolsky and G. R. Gladstone, *J. Geophys. Res.* **101**, 15765 (1996).
22. T. E. Cravens, *Geophys. Res. Lett.* **24**, 105 (1997).
23. V. A. Krasnopolsky, *Bull. Am. Astron. Soc.* **28**, 1095 (1996); *Phys. World* **10**, 21 (1997); *Icarus* **128**, 368 (1997).
24. The emission rate factor for resonant scattering is $g = 0.02654f_l/v$, where f is the oscillator strength and l is the solar radiation in photons $\text{cm}^{-2} \text{ s}^{-1} \text{ Hz}^{-1}$. Values of f are from (41); the solar line intensities at 584 and 304 \AA are from (40). The intensity at 537 \AA is obtained by scaling that at 584 \AA to the line ratio from J. E. Vernazza and E. M. Reeves [Astrophys. J. Suppl. Ser. **37**, 485 (1978)]. The linewidths are taken from (42).
25. The released energy is $E = 1, 0.3$, and -0.02 eV for $\text{M} = \text{H}_2\text{O}, \text{OH},$ and O , respectively. Measurements at 2 keV amu^{-1} in O and O_2 [R. W. McCullough, T. K. McLaughlin, T. Koizumi, H. B. Gilbody, *J. Phys. B* **25**, L193 (1992)] showed total cross sections of 9.3×10^{-17} and $2.7 \times 10^{-16} \text{ cm}^2$ and yields of $\text{He}^+ 304 \text{ \AA}$ of 0.92 and 0.8 , respectively. We expect a lower yield for low ion energies ($\sim 0.1 \text{ keV amu}^{-1}$) in comets.
26. M. B. Shah and H. B. Gilbody, *J. Phys. B* **7**, 256 (1974).
27. We have found neither observations nor theory for this yield. A classic approach [H. Ryufuku, K. Sasaki, T. Watanabe, *Phys. Rev. A* **21**, 745 (1980)] predicts a mean value $n = 1.6$ for He formed in charge transfer of He^{2+} . (This approach is more applicable to one-electron capture.) Therefore, we assume yields of $0.5, 0.33$, and 0.17 for $n = 1, 2, 3$ ($n = 1$ is the He ground state; $n = 2$ and 3 radiate 584 and 537 \AA , respectively).
28. The products of charge transfer keep the velocities of the reactants, $\sim 100 \text{ km s}^{-1}$ for solar wind ions in comets [B. E. Goldstein *et al.*, *Astron. Astrophys.* **187**, 174 (1987)]. This velocity exceeds Doppler velocities corresponding to the solar linewidth, $\sim 40 \text{ km s}^{-1}$ for He and

He^+ lines. Resonant scattering at 100 km s^{-1} is weaker by a factor of $\exp[(100/40)^2] = 500$ than that at low velocities. At least one more collision is necessary to reduce velocity. Each collision of He^+ results in a further charge transfer. Therefore, resonant scattering of $\text{He}^+ 304 \text{ \AA}$ should not occur in comets. Resonant scattering of $\text{He} 537 \text{ \AA}$ is not effective because of the low emission rate factor. The total charge transfer rate is then $3 \times (2 \times 10^{25})/0.17 \approx 3 \times 10^{26} \text{ s}^{-1}$ from He 537 \AA and $<1.5 \times (7 \times 10^{25})/0.5 \approx 2 \times 10^{26} \text{ s}^{-1}$ from $\text{He}^+ 304 \text{ \AA}$. All these evaluations are rather uncertain, and we will use $Q_{\text{He}} \approx 2 \times 10^{26} \text{ s}^{-1}$. Because 1/3 of this value represents two-electron capture, and 1/3 of such captures produce 584 \AA photons, prompt excitation of He 584 \AA is $2 \times 10^{25} \text{ photons s}^{-1}$, and $10^{26} \text{ photons s}^{-1}$ of He 584 \AA refers to resonant scattering. The photon production rate for resonant scattering is $\pi g \rho Q_{\text{He}} / (2vr^2) = 1.3 \times 10^{26} \text{ photons s}^{-1}$, close to the above value.

29. N. C. Wickramasinghe and F. Hoyle, *Astrophys. Space Sci.* **239**, 121 (1996).
30. R. Bingham, J. M. Dawson, V. D. Shapiro, D. A. Mendis, B. J. Kellett, *Science* **275**, 49 (1997); T. G. Northrop, C. M. Lisse, M. J. Mumma, M. D. Desch, *Icarus* **127**, 246 (1997).
31. R. K. Janev, R. A. Phaneuf, H. T. Hunter, *At. Data Nucl. Data Tables* **40**, 249 (1988); J. M. Hodgkinson, T. K. McLaughlin, R. W. McCullough, J. Geddes, H. B. Gilbody, *J. Phys. B* **28**, L393 (1995); D. Dijkkamp, Yu. S. Gordeev, A. Brazuk, A. G. Drentje, F. J. de Heer, *ibid.* **18**, 737 (1985).
32. The production rate of x-ray photons $Q_x = \pi \rho^2 v_{\text{sw}} n_{\text{He}} k_x / (br^2) = 3 \times 10^{25} \text{ photons s}^{-1}$, where $v_{\text{sw}} = 4 \times 10^7 \text{ cm s}^{-1}$ is the solar wind velocity, $n_{\text{He}} = 5 \times 10^{-3} \text{ cm}^{-3}$ is the heavy ion density at 1 AU, and k_x is the cascading factor (23).
33. To illustrate this dependence, we consider deceleration a of dust by solar radiation pressure. The dust paraboloid apex appears in this process at $\rho = v^2/2a$; v is proportional to $r^{-1/2}$ (13), a is proportional to r^{-2} , and therefore ρ is proportional to r . If charging of small dust and removal by electromagnetic forces are more important, then a lifetime τ associated with these processes is proportional to r^2 , and $\rho = v\tau$ is proportional to $r^{3/2}$.
34. $Q_x = 10^{25} \text{ photons s}^{-1}$ ($\rho = 1.2 \times 10^5 \text{ km}$) and $\rho_B = 3 \times 10^4 \text{ km}$ for x-ray emission in Hyakutake, according to ROSAT observations [C. M. Lisse *et al.*, *Science* **274**, 205 (1996)]. The displacement ratio is 9 ± 4 if we use the ROSAT value of ρ_B .
35. Here, we assume that all of the observed x-ray emission is attributable to small dust scattering. Using the definition of Afp (4), we find $Afp = Q_{\text{ph}} r^2 / (\pi \rho l_0)$, where $Q_{\text{ph}} = Q_x$ is the photon production rate and $l_0 = 8 \times 10^9 \text{ photons cm}^{-2} \text{ s}^{-1}$ is the solar x-ray intensity at 1 AU in a range of 75 to 123 \AA (23), which is close to the full spectral width at half-maximum of DS.
36. Using the formalism of emission rate factor $g = g_0/r^2$, we find $Q_x = g_0 \pi \rho Q / 2v$. This allows us to determine the absolute efficiencies g_0 for both comets and their ratio.
37. M. J. Mumma, V. A. Krasnopolsky, M. J. Abbott, *IAU Circular* 6696 (1997).
38. M. J. Mumma *et al.*, *Science* **272**, 1310 (1996); R. L. Millis, D. G. Schleicher, S. M. Lederer, D. J. Osip, *Bull. Am. Astron. Soc.* **28**, 1095 (1996).
39. H. A. Weaver *et al.*, *Science* **275**, 1900 (1997).
40. M. F. A'Hearn, R. L. Millis, D. G. Schleicher, D. J. Osip, P. V. Birch, *Icarus* **118**, 223 (1995).
41. A. I. F. Stewart, *Astron. Astrophys.* **187**, 369 (1987).
42. P. G. Richards, J. A. Fennelly, D. G. Torr, *J. Geophys. Res.* **99**, 8981 (1994).
43. D. R. Lide, Ed., *CRC Handbook of Chemistry and Physics* (CRC Press, Boca Raton, FL, 1995).
44. R. R. Meier, *Space Sci. Rev.* **58**, 1 (1991).
45. We thank T. C. Owen for helpful discussions and T. R. Reyes for software consultations. O. Hainaut and J. Bauer assisted in acquisition of the optical image of Hale-Bopp, which was partially supported by NASA grant NAGW 5015 and NSF grant AST 92-21318 to K. J. Meech. This work was supported by the NASA EUVE Guest Observer Program and the NASA Planetary Astronomy Program through a National Research Council grant to V.A.K. and under contract 196-41-54 to M.J.M.

21 April 1997; accepted 30 June 1997